NANO LETTERS

pubs.acs.org/NanoLett

Enhanced Thermoelectric Metrics in Ultra-long Electrodeposited PEDOT Nanowires

David K. Taggart, Yongan Yang, Sheng-Chin Kung, Theresa M. McIntire, and Reginald M. Penner*

Department of Chemistry, University of California, Irvine, California 92697-2025, United States

ABSTRACT The Seebeck coefficient, S, and the electrical conductivity, σ, of electrodeposited poly(3,4-ethylenedioxythiophene) (PEDOT) nanowires and thin films are reported. PEDOT nanowires were prepared by electropolymerizing 3,4-ethylenedioxythiophene (EDOT) in aqueous $LiClO_4$ within a template prepared using the lithographically patterned nanowire electrodeposition (LPNE) process. These nanowires were 40−90 nm in thickness, 150−580 nm in width, and 200 μm in length. σ and S were measured from 190 K to 310 K by fabricating heaters and thermocouples on top of arrays of 750 PEDOT nanowires. Such PEDOT nanowire arrays consistently produced S values that were higher than those for PEDOT films: up to −122 μV/K (310 K) for nanowires and up to −57 μV/K (310 K) for films. The sample-to-sample variation in S for 14 samples of PEDOT nanowires and films, across a wide range of critical dimensions, is fully explained by variations in the carrier concentrations in accordance with the Mott equation. In spite of their higher $|S|$ values, PEDOT nanowires also had higher σ than films, on average, because electron mobilities were greater in nanowires by a factor of 3.

KEYWORDS Seebeck coefficient, conductive polymer, lithography, electropolymerization, nanopatterning

The efficiency of a thermoelectric element is determined by its dimensionless figure-of-merit, ZT:[1]

$$ZT = \frac{\sigma T S^2}{\kappa} \quad (1)$$

where σ is the electrical conductivity, S is the Seebeck coefficient, T is the temperature, and κ is the thermal conductivity. On the basis of eq 1, electronically conductive organic polymers are interesting candidates for thermoelectric materials since their κ values of 0.05−0.6 W m^{-1} K^{-1} (300 K)[2−5] are an order of magnitude or more lower than the values for crystalline thermoelectric materials such as PbSe and Bi_2Te_3,[1] and their σ values are adjustable from metallic to semiconducting values depending on doping.

Polyacetylene (PA) is the conductive organic polymer that has been most intensively studied for thermoelectrics. S values in the range of 8−22 μV/K and σ = 92−10 200 S/cm have been reported[6,7] for heavily doped PA films. A highest value of S = 1077 μV/K was reported for $MoCl_5$-doped PA films by Park et al.;[8] however, these films had low electrical conductivities of 1.5×10^{-3} S/cm. At higher doping levels, corresponding to σ = 5000−11 000 S/cm, S values from 10 to 30 μV/K were measured.[8] This trend (S inversely correlated with σ) is also observed for other conductive polymers,[9] but as compared with PA, other electronically conductive polymers have yielded lower S values and lower σ in general.[10−13] For example, polyaniline films produce S = ∼3 μV/K and σ = 15−20 S/cm (300 K),[11] and polypyrrole films showed S = 6−7.5 μV/K with σ = 100−3000 S/cm.[10] An exception to this generalization is recent work from Katz and co-workers[14] who found that extremely high S values, up to 700 μV/K, can be produced for functionalized polythiophenes by blending these polymers with hole-stabilizers such as tetra-fluorotetracyanoquinodimethane (F4TCNQ), but the σ values for the resulting polymer blends were ≤0.00017 S/cm. The extremely high σ values achievable for heavily doped PA films translate into power factors, $S^2\sigma$, of ∼10^{-3} W m^{-1} K^{-1}, 2 orders of magnitude higher than those for other polymers in spite of the relatively low S values for these materials (Table 1).

The thermoelectric properties of poly(3,4-ethylenedioxythiophene) (PEDOT) have also been investigated, but up until now these studies have been limited to mixtures of PEDOT with poly(styrenesulfonate) (PSS), which renders the oxidized form of the polymer water-soluble (PEDOT:PSS). Typical values for S have been in the range of 12−16 μV/K for PEDOT:PSS films[15] or pellets[16] with $\sigma \leq$ 60 S/cm (300 K). Chang et al.[17] reported an S value of 888 μV/K for a PEDOT:PSS film with σ = 0.06 S/cm (300 K), but for 13 other samples with σ > 0.5 S/cm, S was 41 μV/K or below. Kim et al.[18] showed that a successful strategy for increasing σ without depressing S involved mixing PEDOT:PSS with carbon nanotubes. Films of these two-component mixtures had high σ values of 100−400 S/cm while showing S values as high as 41 μV/K (300 K) for 1:1 mixtures based on weight. Tritt and co-workers predicted[19] that even higher S values approaching 100 μV/K should be achievable for polythiophene and its derivatives based upon the favorable band structures of these polymers. Duvail and co-workers synthesized and studied nanowires of PEDOT−ClO_4^-, observing

* To whom correspondence should be addressed. E-mail: rmpenner@uci.edu.
Received for review: 08/24/2010
Published on Web: 00/00/0000

DOI: 10.1021/nl103003d | *Nano Lett.* **XXXX,** *xxx,* 000–000

TABLE 1. Experimentally Measured σ, S, and $S^2\sigma$ for PEDOT Nanowires and Films and Comparison with Literature Values for PEDOT and Other Conductive Polymers

	σ S/cm		S μV/K		$S^2 \cdot \sigma$ W·m^{-1}·K^{-2}		μ cm^2·V^{-1} s^{-1}	
sample	310 K	300 K	310 K	300 K	310 K	300 K	310 K	reference
PEDOT Nanowires Height × Width								
48 nm × 582 nm	40.5	39.6	−38	−33	5.8×10^{-6}	4.3×10^{-6}	9.4	this work
80 nm × 440 nm	12.0	11.7	−85	−80	8.7×10^{-6}	8.4×10^{-6}	11.4	”
90 nm × 205 nm	7.9	7.6	−122	−69	1.2×10^{-5}	3.6×10^{-6}	12.5	”
60 nm × 340 nm	6.9	6.6	−42	−38	1.2×10^{-6}	9.6×10^{-7}	2.0	”
66 nm × 568 nm			−70	−76				”
40 nm × 245 nm			−80	−78				”
40 nm × 251 nm			−35	−40				”
40 nm × 258 nm			−91	−73				”
60 nm × 157 nm			−104	−75				”
75 nm × 172 nm			−44	−39				”
mean values	16.8	16.4	−74	−62	9.2×10^{-6}	6.3×10^{-6}	9 ± 5	”
PEDOT Films Height × Width								
30 nm × 1.5 mm	18.3	17.9	−34	−33	2.1×10^{-6}	2.0×10^{-6}	2.4	this work
150 nm × 180 μm	13.2	13.0	−57	−47	4.4×10^{-6}	2.9×10^{-6}	4.2	”
45 nm × 1.5 mm	9.7	9.3	−55	−57	2.9×10^{-6}	3.0×10^{-6}	3.8	”
170 nm × 312 μm	3.2	3.1	−44	−39	6.3×10^{-7}	4.7×10^{-7}	0.54	”
mean values	11.1	10.9	−48	−44	2.6×10^{-6}	2.1×10^{-6}	3 ± 2	”
Literature Values (all data 300 K)								
PA iodine doped thickness, t = 300 nm	3×10^4 to 5×10^4		15−20		1.2×10^{-3} to 1.5×10^{-3}			7
PA metal- Cl_5 doped	$0.15-1.1 \times 10^4$		11−1077		1.2×10^{-7} to 1.5×10^{-3}			8
PA $FeCl_3$ or I doped t = 9 − 35 μm	$92-1 \times 10^4$		9−22		6.2×10^{-7} to 8.3×10^{-5}			6
polyaniline in PETG or PMMA	0.13−30		3−9		6.4×10^{-11} to 2.2×10^{-7}			11
polypyrrole films t = 40 − 100 μm	26		7		1.7×10^{-7}			10
doped poly(alkylthiophene) t = 1.75 − 3 μm	0.00002−0.0013		200−700		1.0×10^{-10} to 8.8×10^{-9}			14
polythiophene films t = sub 20 μm	0.00005−3		20−10 000		5.0×10^{-8} to 1.0×10^{-5}			12
polycarbazole and derivatives	0.00027−0.29		4.9−127		5.0×10^{-10} to 1.5×10^{-7}			13
PEDOT/PSS DMSO-treated	0.06−220		12−888		1.6×10^{-9} to 4.8×10^{-6}		0.49−2.11	17
PEDOT/PSS pellets DMSO-treated	9−54		12−15		2.0×10^{-7} to 8.3×10^{-7}			16
PEDOT/PSS films t = 10 − 30 μm	0.80−80		9−12		1.2×10^{-8} to 8.0×10^{-7}			15
PEDOT/PSS:carbon nanotube composite films; t = 0.07 − 13 mm	0.20−0.40		10000−40000		1.0×10^{-6} to 2.5×10^{-5}			18

that the σ of these nanowires increased from 10 to 400 S/cm as the wire diameter was decreased from 200 nm to 20−40 nm, but S was not measured in that work.[20] Here we describe the preparation of arrays of PEDOT nanowires that simultaneously exhibit electrical conductivities of ∼7−40 S/cm and n-type Seebeck coefficients up to $|122|$ μV K^{-1} at 310 K. These S values are higher than those we have measured for PEDOT films (S = 34−57 μV/K), prepared using an identical electrodeposition procedure, possibly as a consequence of a lower carrier concentration in these PEDOT nanowires as compared with films. However, in spite of these lower carrier concentrations, the electrical conductivity of the PEDOT nanowires is significantly higher than in PEDOT films prepared using an identical electrodeposition procedure because of enhanced electron mobilities in the nanowires.

Previously, nanowires of electronically conductive polymers have been prepared using a variety of methods including electrodeposition,[21−25] self-assembly in porous anodic alumina templates,[26] electrodeposition into polycarbonate templates,[20,27−30] electrospinning,[31−33] and various other techniques.[34−38] Here, we have adapted the lithographically patterned nanowire electrodeposition (LPNE) method[39−41] to fabricate arrays of PEDOT nanowires on thermally conductive Si_3N_4 -coated silicon substrates. LPNE leverages conventional microfabrication methods to produce a horizontal trench with a width of ∼600 nm terminated by a vertical nickel electrode (Figure 1a). Immersion of this trench into an aqueous solution of 3,4-ethylenedioxythiophene (EDOT) (2.5 mM EDOT, 12.5 mM $LiClO_4$, in Millipore water) permitted growth of a PEDOT nanowire by oxidative electropolymerization at the nickel electrode and within the

DOI: 10.1021/nl103003d | *Nano Lett.* **XXXX,** *xxx,* 000−000

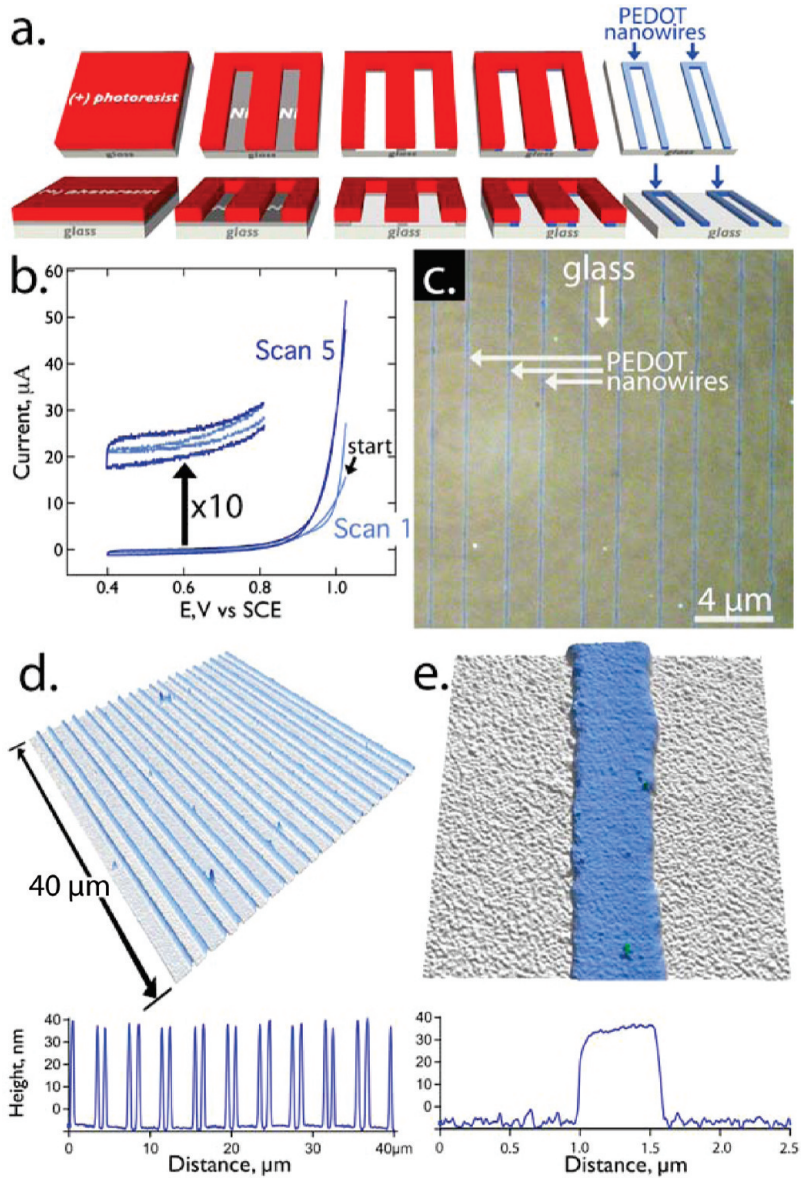

FIGURE 1. Synthesizing arrays of PEDOT nanowires using LPNE: (a) Five-step process flow for the synthesis of PEDOT nanowires using the LPNE method. (i) a nickel layer and a (+)-photoresist (PR) layer are both deposited on a glass surface. (ii) The PR layer is patterned with a contact mask, (iii) nickel is etched from the patterned surface using nitric acid. (iv) PEDOT is deposited by anodic electropolymerization from an aqueous solution containing EDOT. PEDOT is deposited at the nickel electrodes, within the horizontal trench delineated on three sides by the PR, the glass surface, and the nickel electrodes. (v) PR and nickel are selectively removed using acetone and 0.8 M nitric acid, respectively, to expose the PEDOT nanowires. (b) Current versus voltage plots (cyclic voltammograms) for the electropolymerization of EDOT to form PEDOT nanowires within an LPNE template. The synthesis solution contains 2.5 mM EDOT and 12.5 mM $LiClO_4$ in Millipore water, and the voltage scan rate is 20 mV/s. The oxidative polymerization reaction occurring at positive potential is $n(C_6H_6O_2S) + \gamma n ClO_4^- \rightarrow [C_6H_4O_2S]_n(ClO_4^-)_{\gamma n} + 2nH^+ + 2ne^-$, where γ is the fractional positive charge per monomer unit. (c) Brightfield optical micrograph of PEDOT nanowire pattered on glass. (d) Atomic force microscope (AFM) image of an array of 40 × 200 nm PEDOT nanowires on glass. A height versus distance trace across these nanowires is shown at bottom. (e) High magnification AFM image of a 40 × 600 nm PEDOT nanowire on glass. A height versus distance trace across this nanowire is shown at bottom.

confines of this trench (Figure 1b). This method provided for independent control over the thickness and width of the nanowire while also enabling the synthesis of PEDOT nanowires that were millimeters in total length.

The thickness of PEDOT nanowires matched the thickness of the nickel layer employed in the LPNE process, as indicated by AFM measurements of the nanowire (Figure 1d,e). The width of PEDOT nanowires was controlled using the number of electrodeposition scans (Figure 1b): The initial scan between an initial voltage of +1.05 V to +0.4 V vs saturated calomel electrode (SCE) at 20 mV/s produced no detectable PEDOT electrodeposition, while the second voltametric scan produced PEDOT nanowires with a width of 144 ± 10 nm. Subsequent scans added increments of this width to the nascent nanowire. PEDOT films on nickel were electrodeposited using the same solution and procedure as

DOI: 10.1021/nl103003d | *Nano Lett.* **XXXX,** *xxx,* 000–000

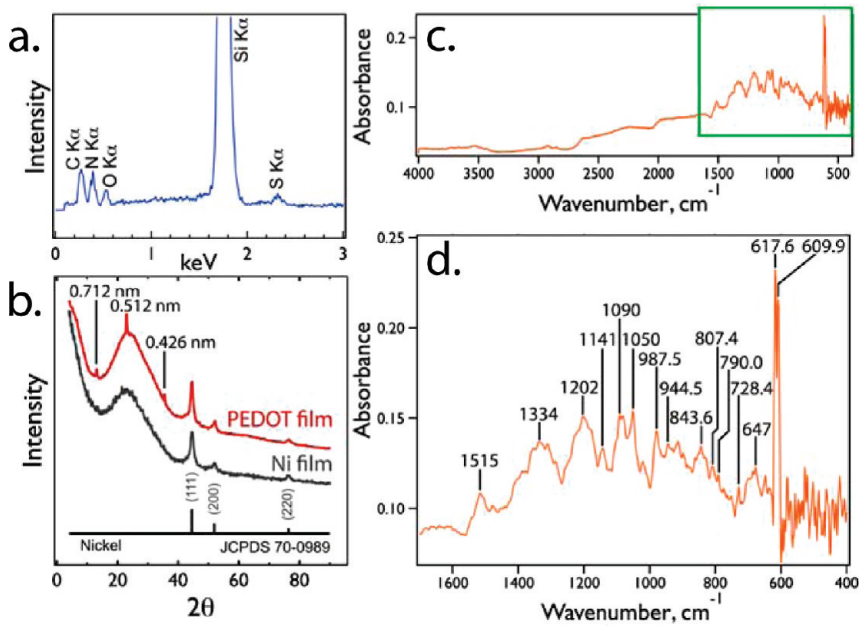

FIGURE 2. Characterization of PEDOT nanowires: (a) EDX spectrum of PEDOT nanowires on glass. (b) GIXRD spectrum of PEDOT film (thickness = 200 nm) on glass. Three reflections attributable to PEDOT (*d*-spacings indicated) are observed at 13.2°, 23.0°, and 35.5°. (c,d) Fourier transfer infrared (FTIR) absorption spectra for PEDOT nanowires on silicon. This transmission mode spectrum was acquired using a FTIR spectrometer (Avatar 370, Thermo Electron Corporation Madison, WI) equipped with a KBr beam splitter and a high-temperature ceramic source. Five double-side polished silicon wafers on which PEDOT nanowires had been deposited at 2 μm pitch, (a total of 10 surfaces) were mounted at 74° from normal incidence (Si Brewster angle) in thin slots in a Teflon holder within a glass cell of 11 cm path length enclosed with 32 mm diameter ZnSe windows. FTIR spectra acquired as single beams at 4 cm^{-1} resolution with a liquid nitrogen-cooled mercury cadmium telluride detector (MCT-A). Absorbance spectra were obtained by ratioing sample single beam spectra for PEDOT-treated Si (4000 scans) to the background spectrum of clean silicon (2048 scans). Band assignments are indicated in Table 2.

PEDOT nanowires. Electrodeposited PEDOT thin films are a light blue color, the color of oxidized PEDOT.[42−45] When PEDOT nanowires approach a micrometer in width and height, this blue color can be seen in optical micrographs (Figure 1c).

Energy dispersive X-ray (EDX) spectroscopy was used to qualitatively confirm the elemental composition of the PEDOT films (Figure 2a). Signals for five elements are observed: Si and N from the Si_3N_4 substrate, and C, O, and S, the elemental constituents of PEDOT ($(C_6 H_6 O_2S)_n$). To quantitatively confirm that the electrodeposited nanowires were PEDOT, infrared (IR) transmission spectra were acquired for arrays of nanowires prepared using our procedure. To achieve spectra of high signal-to-noise, five samples with PEDOT nanowires were patterned at a 2 μm pitch. In these IR spectra (Figure 2c,d), 14 peaks can be assigned to PEDOT (Table 2) showing conclusively that the electrodeposited nanowires are composed of PEDOT. We also examined PEDOT nanowires and films using grazing incidence X-ray diffraction (GIXRD), but nanowires were completely amorphous while PEDOT films showed reflections at $2\theta = 13.2°$, 23° and 35.5° (Figure 2b). We report this XRD pattern in spite of the fact that consensus diffraction assignments for PEDOT have not yet been reported in the literature.

To measure S and σ for PEDOT nanowires, an array of ~750 nanowires plus a single "orphaned" nanowire were patterned by LPNE onto a Si_3N_4 (400 nm) coated Si wafer

TABLE 2. Band Assignments For the Transmission Infrared Absorption Spectrum of PEDOT Nanowires Shown in Figure 2d

peak, cm^{-1}	assignment	reference
2950	asymmetric ν (C−H)	48
2860	symmetric ν (C−H)	48
1515	ν (C═C)	49−51
1334	C−C or C═C	51, 52
1202	ν (C−O−C)	48
1141	ν (C−O−C)	49−52
1090	ν (C−O−C)	49−52
1050	ν (C−O−C)	49−51
979	ν (C−S)	51, 52
945	ν (C−S)	49, 50
844	ν (C−S)	49−52
807	Si	53
790	γ (C−S)	49, 50
728	δ (C−S)	49, 50
677	δ (C−S)	49, 50, 52
618	Si	52
610	Si	52

(Figure 3a,b). Using five additional processing steps, two meander heaters and two Ag/Ni thermocouples were fabricated on top of this nanowire array (Figure 3c), providing the ability to heat the array from either side while simultaneously measuring the mean temperature and the difference in temperature, ΔT, across a 200 μm length segment of these wires. A high thermal conductivity of the support for the device is important because the mean temperature of the nanowires is controlled by thermostatting a brass stage upon which this device is supported within a vacuum cry-

DOI: 10.1021/nl103003d | *Nano Lett.* **XXXX,** *xxx,* 000−000

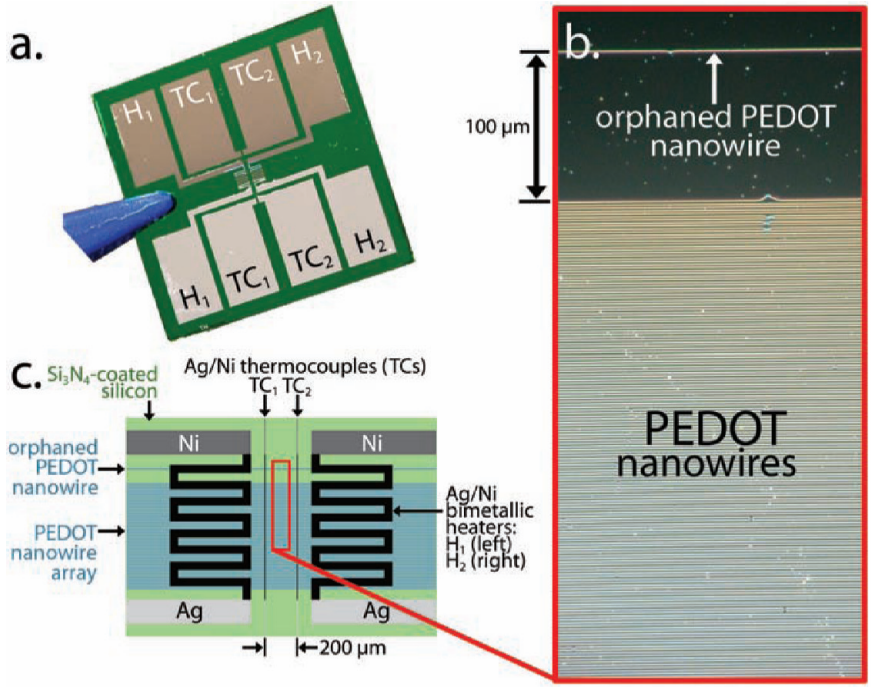

FIGURE 3. (a) Photograph of device chip employed for measurements of S and σ with integrated heaters (H_1 and H_2), thermocouples (TC_1 and TC_2) and PEDOT nanowire array. (b) A dark field optical micrograph showing a PEDOT nanowire array and the orphaned PEDOT nanowire in a typical device. (c) Schematic diagram showing the chip layout for the device shown in (a).

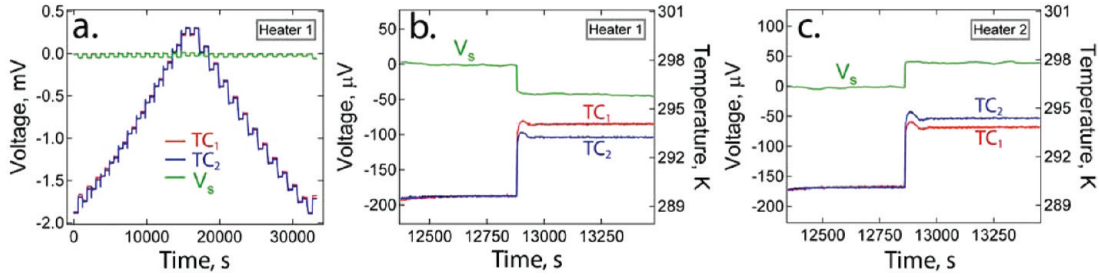

FIGURE 4. (a) Raw S versus time data using H_1, each step corresponds to a 10 K jump in temperature starting at 190 K and peaking at 310 K. (b) Zoom in of the step at 290 K showing positive V_s. (c) At the same temperature of 290 K, the sign of the V_s is inverted when H_2 is instead activated.

ostat, and expeditious measurements of S and σ across a range of temperatures requires that the device remains in rapid thermal equilibrium. For this reason, wafers consisting of an electrically insulating silicon nitride (Si_3N_4) layer (thickness = 400 nm) on [100] silicon (thickness = 670 μm) was used as the support in preference to glass because the thermal conductivity is more than 100 times higher. In this device configuration, the electrical contacts employed for measurement of the Seebeck voltage, V_s, are the same as those of the two thermocouples (TC_1 and TC_2) involved in the measurement of the temperature, and this confers the advantage that the temperature measurement occurs precisely at the point of electrical contact to the nanowires. The σ of PEDOT nanowires having particular lateral dimensions was measured using the single, orphaned nanowire using four electrical contacts with separate application of current and measurement of voltage. The use of the orphaned nanowire is required because it is impossible to know how many of the 750 PEDOT nanowires in our array are electrically continuous, so the electrical conductivity of these nanowires can not be extrapolated from electrical measurements on this nanowire array. Instead, we pattern a single "orphaned" nanowire adjacent to the array. It's electrical conductivity is assumed to accurately approximate that of the electrically continuous members of the array.

After placing this device on the brass stage of a vacuum cryostat (base pressure = 5×10^{-6} Torr), S was measured at each of 13 temperature points from 190 K to 310 K in 10 K intervals (Figure 4a). After equilibration at each temperature point, one of the heaters was powered by a constant current (30−300 mA), while the temperature at the two TCs (calibrated prior to use) together with the resulting Seebeck voltage, V_s, developed between the two thermocouples, were measured as a function of time (Figure 4b). At the 290 K

DOI: 10.1021/nl103003d | Nano Lett. XXXX, xxx, 000–000

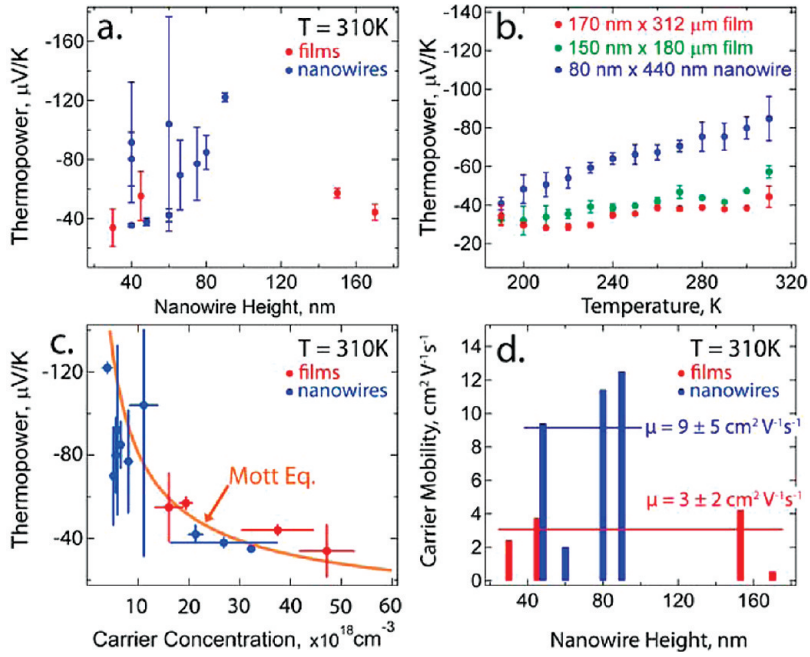

FIGURE 5. (a) Measured *S* versus nanowire height for PEDOT nanowires and films at 310 K. (b) *S* versus temperature over the range from 190 K to 310 K. Error bars represent $\pm 1\sigma$ for 2−4 measurements at each temperature point. (c) *S* versus carrier concentration fitted with the Mott relation (eq 2). (d) Electron mobilities versus the film or nanowire height, showing also (horizontal line) the mean mobility value.

temperature point, for example (Figure 4b), activation of heater H_1 produced an increase at both TC_1 and TC_2, with a $\Delta T = 0.74$ K and an induced Seebeck voltage, $V_s = -31$ μV. *S* was then calculated as $S = V_s/\Delta T$. For both films and nanowires, the sign of V_s was opposite to that of ΔT (voltage (+) at the hot contact), indicating that majority carriers are electrons. Activating heater H_2 inverted the temperature gradient (Figure 4c) and the sign on V_s, which was -30 μV in this trial. Four measurements of *S* were acquired at each of 13 temperature points from 190 K to 310 K, and the error bars in Figure 5a,b,c represent $\pm 1\sigma$ based on these measurements.

The *S* for PEDOT nanowires ranged from -35 μV/K to -122 μV/K at 310K, where the average value for the nine measured nanowire samples is -74 ± 31 μV/K. The values at 300 K ranged from -80 μV/K to -34 μV/K with an average value of -62 ± 20 μV/K. As compared with prior measurements of *S* for conductive polymers (Table 1), these values are higher than prior measurements for PEDOT but lower than the highest values that have been seen at PA and polythiophene derivatives. We measured lower values of *S* for PEDOT films which produced values ranging from -57 μV/K to -34 μV/K at 310 K and -47 μV/K to -33 μV/K at 300 K. The average value for four PEDOT films is -48 ± 11 μV/K at 310 K and -44 ± 10 μV/K at 300 K.

To first order, measured values of *S* were uncorrelated with nanowire or film height, the smallest dimension of these structures, across the height range from 30 nm to 170 nm (Figure 5a). However $|S|$ increased in direct proportion to *T* for both PEDOT thin films and nanowires (Figure 5b). This behavior is in accord with the predictions of the Mott relation:[46]

$$S = \frac{\pi^2 k^2 m^* T}{(3\pi^2)^{2/3}\hbar |e| n^{2/3}} \qquad (2)$$

where m^* is the effective mass of majority carriers and *n* is the carrier concentration (cm^{-3}). From the slope of the measured *S* versus *T* plot (Figure 5b) and using the accepted values of $m^* = 0.121 m_e$ for PEDOT,[47] *n* estimated in this way ranged from 4.0×10^{18} cm^{-3} to 45×10^{18} cm^{-3}. As shown clearly by Figure 5c, the elevation of *S* at 310 K for PEDOT nanowires can be accounted for by lower carrier concentrations in PEDOT nanowires as compared with films. These lower *n* values would be expected to depress the σ of nanowires as compared with films but, in fact, the opposite is observed (Table 1): σ values for PEDOT nanowires are 50% higher than the measured σ for films. The mitigating factor is the electron mobility, μ, which is a factor of 3 higher in PEDOT nanowires than in films, on average (Figure 5d, Table 1). This elevated electron mobility is the key factor distinguishing the thermoelectric performance of PEDOT nanowires and films. The microscopic origin for this effect is not apparent from the data we have presented here, and it has not been documented by the prior measurements on conductive polymer nanowires to our knowledge. Duvail et al.[20] observed a strong enhancement in the σ (300 K) of PEDOT−ClO_4^- nanowires with decreasing wire diameter over the range from 200 nm to 20 nm, but the carrier

DOI: 10.1021/nl103003d | *Nano Lett.* **XXXX,** *xxx,* 000–000

concentration in these nanowires was not determined, and it is therefore unknown whether this effect originates in an elevation of μ or n.

With PEDOT nanowires prepared by LPNE, we have achieved power factors ($S^2\sigma$) up to 9.2×10^{-5} W m^{-1} K^{-1} that equal or exceed those reported in all previous studies of conductive polymers (Table 1) with the exception of devices based upon PA. These power factors are higher for PEDOT nanowires as compared to films by exactly the same factor of 3 as the electron mobilities. The origin of the elevated electron mobilities seen in these PEDOT nanowires is not addressed by the data we have reported here. However, the implication is that the orientational order of PEDOT chains and/or the crystallinity of the polymer within these nanowires differs significantly from the corresponding properties of thin films. The detailed atomic scale structure of these nanomaterials is a topic for further study.

Acknowledgment. The double-side polished silicon wafers used for the FTIR experiments were kindly provided by Dr. Mark Dishner, Dr. Satya Kurada, and Dr. Qiguang Li at KLA-Tencor. T.M.M. thanks Dr. John N. Russell, Jr. at the Naval Research Laboratories for valuable discussions. This work was supported by the National Science Foundation Grant DMR-0654055, the Petroleum Research Fund of the American Chemical Society 46815-AC 10, and the UCI School of Physical Sciences Center for Solar Energy.

REFERENCES AND NOTES

(1) Rowe, D. M. *CRC Handbook of Thermoelectrics*; CRC Press: Boca Raton, FL, 1995.
(2) Yan, H.; Ohno, N.; Toshima, N. *Chem. Lett.* **2000**, 392–393.
(3) Yan, H.; Sada, N.; Toshima, N. *J. Therm. Anal. Calorim.* **2002**, *69*, 881–887.
(4) de Albuquerque, J.; Melo, W.; Faria, R. *Rev. Sci. Instrum.* **2003**, *74*, 306–308.
(5) Kaul, P. B.; Day, K. A.; Abramson, A. R. *J. Appl. Phys.* **2007**, *101*, 083507-1–083507-7.
(6) Pukacki, W.; Plocharshi, J.; Roth, S. *Synth. Met.* **1994**, *62*, 253–256.
(7) Nogami, Y.; Keneko, H.; Ishiguro, T.; Takahashi, A.; Tsukamoto, J.; Hosoito, N. *Solid State Commun.* **1990**, *76*, 583–586.
(8) Park, Y. *Synth. Met.* **1991**, *45*, 173–182.
(9) Mateeva, N.; Niculescu, H.; Schlenoff, J.; Testardi, L. *J. Appl. Phys.* **1998**, *83*, 3111–3117.
(10) Maddison, D.; Unsworth, J.; Roberts, R. *Synth. Met.* **1988**, *26*, 99–108.
(11) Subramaniam, C.; Kaiser, A.; Gilberd, P.; Liu, C.; Wessling, B. *Solid State Commun.* **1996**, *97*, 235–238.
(12) Hiraishi, K.; Masuhara, A.; Nakanishi, H.; Oikawa, H.; Shinohara, Y. *Jpn. J. Appl. Phys.* **2009**, *48*, 071501.
(13) Wakim, S.; Aich, B.-R.; Tao, Y.; Leclerc, M. *Polym. Rev.* **2008**, *48*, 432–462.
(14) Sun, J.; Yeh, M.-L.; Jung, B. J.; Zhang, B.; Feser, J.; Majumdar, A.; Katz, H. E. *Macromolecules* **2010**, *43*, 2897–2903.
(15) Kim, J.; Jung, J.; Lee, D.; Joo, J. *Synth. Met.* **2002**, *126*, 311–316.
(16) Jiang, F. X.; Xu, J. K.; Lu, B. Y.; Xie, Y.; Huang, R. J.; Li, L. F. *Chin. Phys. Lett.* **2008**, *25*, 2202–2205.
(17) Chang, K.-C.; Jeng, M.-S.; Yang, C.-C.; Chou, Y.-W.; Wu, S.-K.; Thomas, M. A.; Peng, Y.-C. *J. Electron. Mater.* **2009**, *38*, 1182–1188.
(18) Kim, D.; Kim, Y.; Choi, K.; Grunlan, J. C.; Yu, C. *ACS Nano* **2010**, *4*, 513–523.
(19) Gao, X.; Uehara, K.; Klug, D.; Patchkovskii, S.; Tse, J.; Tritt, T. *Phys. Rev. B* **2005**, *72*, 125202.
(20) Duvail, J. L.; Long, Y.; Cuenot, S.; Chen, Z.; Gu, C. *Appl. Phys. Lett.* **2007**, *90*, 102114.
(21) Liu, R.; Lee, S. B. *J. Am. Chem. Soc.* **2008**, *130*, 2942–2943.
(22) Park, D. H.; Kim, H. S.; Lee, Y. B.; Ko, J. M.; Lee, J.-Y.; Kim, H.-J.; Kim, D.-C.; Kim, J.; Joo, J. *Synth. Met.* **2008**, *158*, 90–94.
(23) Dan, Y.; Cao, Y.; Mallouk, T. E.; Johnson, A. T.; Evoy, S. *Sens. Actuators, B: Chem.* **2007**, *125*, 55–59.
(24) Xiao, R.; Il Cho, S.; Liu, R.; Lee, S. B. *J. Am. Chem. Soc.* **2007**, *129*, 4483–4489.
(25) Joo, J.; Kim, B.; Park, D.; Kim, H.; Seo, D.; Shim, J.; Lee, S.; Ryu, K.; Kim, K.; Jin, J.; Lee, T.; Lee, C. *Synth. Met.* **2005**, *153*, 313–316.
(26) Yang, Y.; Jiang, Y.; Xu, J.; Yu, J. *Mater. Sci. Eng. B: Solid State Mater. Adv. Technol.* **2007**, *139*, 251–255.
(27) Long, Y. Z.; Duvail, J. L.; Chen, Z. J.; Jin, A. Z.; Gu, C. Z. *Polym. Adv. Technol.* **2009**, *20*, 541–544.
(28) Long, Y.-Z.; Yin, Z.-H.; Li, M.-M.; Gu, C.-Z.; Duvail, J.-L.; Jin, A.-Z.; Wan, M.-X. *Chin. Phys. B* **2009**, *18*, 2514–2522.
(29) Duvail, J.; Retho, P.; Fernandez, V.; Louarn, G.; Molinie, P.; Chauvet, O. *J. Phys. Chem. B* **2004**, *108*, 18552–18556.
(30) Orgzall, I.; Lorenz, B.; Ting, S.; Hor, P.; Menon, V.; Martin, C.; Hochheimer, H. *Phys. Rev. B* **1996**, *54*, 16654–16658.
(31) Liu, H.; Kameoka, J.; Czaplewski, D.; Craighead, H. *Nano Lett.* **2004**, *4*, 671–675.
(32) Chronakis, I.; Grapenson, S.; Jakob, A. *Polymer* **2006**, *47*, 1597–1603.
(33) Laforgue, A.; Robitaille, L. *Macromolecules* **2010**, *43*, 4194–4200.
(34) Chen, Y.; Luo, Y. *Adv. Mater.* **2009**, *21*, 2040–2044.
(35) Hamedi, M.; Herland, A.; Karlsson, R. H.; Inganas, O. *Nano Lett.* **2008**, *8*, 1736–1740.
(36) Samitsu, S.; Iida, T.; Fujimori, M.; Heike, S.; Hashizume, T.; Shimomura, T.; Ito, K. *Synth. Met.* **2005**, *152*, 497–500.
(37) Wang, Y.; Coti, K. K.; Jun, W.; Alam, M. M.; Shyue, J.-J.; Lu, W.; Padture, N. P.; Tseng, H.-R. *Nanotechnology* **2007**, *18*, 424021.
(38) Lu, H.-H.; Lin, C.-Y.; Hsiao, T.-C.; Fang, Y.-Y.; Ho, K.-C.; Yang, D.; Lee, C.-K.; Hsu, S.-M.; Lin, C.-W. *Anal. Chim. Acta* **2009**, *640*, 68–74.
(39) Xiang, C.; Yang, Y.; Penner, R. M. *Chem. Commun.* **2009**, 859–873.
(40) Xiang, C.; Kung, S.-C.; Taggart, D. K.; Yang, F.; Thompson, M. A.; Gueell, A. G.; Yang, Y.; Penner, R. M. *ACS Nano* **2008**, *2*, 1939–1949.
(41) Menke, E. J.; Thompson, M. A.; Xiang, C.; Yang, L. C.; Penner, R. M. *Nat. Mater.* **2006**, *5*, 914–919.
(42) Duluard, S.; Ouvrard, B.; Celik-Cochet, A.; Campet, G.; Posset, U.; Schottner, G.; Delville, M. H. *J. Phys. Chem. B* **2010**, *114*, 7445–7451.
(43) Lock, J. P.; Lutkenhaus, J. L.; Zacharia, N. S.; Im, S. G.; Hammond, P. T.; Gleason, K. K. *Synth. Met.* **2007**, *157*, 894–898.
(44) Pacios, R.; Marcilla, R.; Pozo-Gonzalo, C.; Pomposo, J. A.; Grande, H.; Aizpurua, J.; Mecerreyes, D. *J. Nanosci. Nanotechnol.* **2007**, *7*, 2938–2941.
(45) Cutler, C.; Bouguettaya, M.; Kang, T.; Reynolds, J. *Macromolecules* **2005**, *38*, 3068–3074.
(46) Cutler, M.; Leavy, J.; Fitzpatrick, R. *Phys. Rev.* **1964**, *133*, A1143–A1152.
(47) Pai, C.; Liu, C.; Chen, W.; Jenekhe, S. *Polymer* **2006**, *47*, 699–708.
(48) Pavia, D. L.; Lampman, G. M.; Kriz, G. S. *Introduction to Spectroscopy: A Guide for Students of Organic Chemistry*, 3rd ed.; Harcourt College Publishers: Fort Worth, TX, 2001.
(49) Kvarnstrom, C.; Neugebauer, H.; Blomquist, S.; Ahonen, H.; Kankare, J.; Ivaska, A. *Electrochim. Acta* **1999**, *44*, 2739–2750.
(50) Kvarnstrom, C.; Neugebauer, H.; Blomquist, S.; Ahonen, H.; Kankare, J.; Ivaska, A.; Sariciftci, N. *Synth. Met.* **1999**, *101*, 66–66.
(51) Seo, K.; Chung, I. *Polymer* **2000**, *41*, 4491–4499.
(52) Choi, J.; Han, M.; Kim, S.; Oh, S.; Im, S. *Synth. Met.* **2004**, *141*, 293–299.
(53) Choi, W.; Lee, M.; Kim, E.; Kim, C.; Min, S.; Park, C.; Lee, J. *Appl. Phys. Lett.* **1996**, *69*, 3402–3404.

DOI: 10.1021/nl103003d | *Nano Lett.* **XXXX,** *xxx,* 000–000